A layered-wise, composite modelling approach for fibre textile reinforced cementitious composites

El Kadi, Michael; Tysmans, Tine; Verbruggen, Svetlana; Vervloet, Jolien; De Munck, Matthias; Wastiels, Jan; Van Hemelrijck, Danny

Published in:
Cement and Concrete Composites

DOI:
10.1016/j.cemconcomp.2018.08.015

Publication date:
2018

A layered-wise, composite modelling approach for fibre textile reinforced cementitious composites

M. El Kadi[1*], T. Tysmans[1], S. Verbruggen[1], J. Vervloet[1], M. De Munck[1], J. Wastiels[1], D. Van Hemelrijck[1]

[1] Vrije Universiteit Brussel (VUB), Department Mechanics of Materials and Constructions, Pleinlaan 2, 1050 Brussels, Belgium

*Corresponding author (michael.el.kadi@vub.be)

Abstract

Textile Reinforced Cements (TRCs) offer an adequate alternative to more conventional building systems in construction due to their tunable and lightweight geometries. TRCs are currently either modelled by means of a discrete approach, where the textiles and the matrix are modelled separately, or by means of a smeared approach that averages the material's mechanical response over the cross-section.

The research presented in this paper proposes a new, layered-wise approach of modelling where the through-thickness response of the composite is subdivided in different layers with individual mechanical properties. A tensile experimental campaign on different combinations of TRC layups, combining both glass and carbon fibre textiles, is performed and used as an input for the layered-wise numerical model. The model is then validated by comparison with flexural experiments performed on four different TRC layup combinations. The good agreement witnessed between the numerical predictions and the experimental results validates the layered-wise modelling approach proposed in this paper.

Keywords: TRC, composite lay-up, smeared model, tension, bending, experimental characterization, numerical model

1. Introduction

The main goal of a composite material is to combine two or more, inherently less performing materials into one material that takes advantage of the mechanical strengths of its components and at the same time bypasses their lacunas. In the case of TRC, the composite material combines a cementitious matrix with a fibre textile reinforcement. The cementitious matrix provides the structural stability and compressive resistance of the composite and serves as a backbone for the fibre textiles. These textiles offer a good tensile resistance and bridge the tensile cracks inside the cementitious matrix, which leads to a more controlled tensile response that is also more ductile than the tensile behaviour of the cementitious matrix on its own [1]–[3]. Another advantage offered by TRCs is the ease at which they can be tuned geometrically towards the application's needs [1], [4]–[7].

In literature, several ways of modelling TRCs are described. When the fibre textiles are present in a discrete manner throughout the TRC section, they lend themselves for discrete modelling approaches [8]–[12]**,** where the fibre textiles are modelled as a separate entity inside the cementitious matrix. However, when the fibre textiles are more uniformly distributed, micromechanical composite models can be applied to describe their mechanical behaviour [13] and smeared modelling approaches are to be preferred [7], [14]–[16]. The main advantage of discrete modelling approaches is their theoretical ability to perfectly match and represent the

composite's mechanical behaviour as well as its fibre-matrix bond. These bond properties and behaviour are however not always easy to characterize experimentally, making them a bottleneck for discrete modelling approaches. On the other hand, smeared models do not have these bond modelling issues since they model the composite as one material, but do not offer the same level of detail or tunability as their discrete counterparts. While the advantages of the smeared modelling approach are widely recognised [17], [15], its disadvantages become more pronounced when considering the tendency towards spaced 3D textiles as reinforcement in TRC [18]–[20]. For these 3D textiles, the distance between the reinforcement layers is significant, and the reinforcement cannot be considered to be uniformly distributed over the cross section; the lever arm and hence the flexural stiffness is not correctly represented in a fully smeared approach.

In this paper a new modelling approach is described which combines the advantages of the previously discussed approaches and subdivides the TRC cross-section into a stacking of different layers according to where the fibre textiles are present throughout the thickness of the composite. Layers are given individual mechanical responses according to the designated layer type. The difference with discrete models is that in the proposed approach the textiles are not modelled individually but instead a thin layer of textile and cement is considered, i.e. a cement-impregnated textile layer. This layered-wise modelling approach distinguishes itself from more traditionally used smeared modelling approaches because it offers the user an efficient and easy to tune model where any cement-impregnated textile layer can effortlessly be interchanged according to the user's wishes and the application's requirements. It also distinguishes itself from discrete modelling approaches since no bond properties have to be inputted. In other words, once all the different cement-impregnated fibre textile layers are mechanically characterized, they can easily be combined in any desired layup combination.

In order to validate the proposed layered-wise modelling approach, TRCs combining two-dimensional glass and carbon fibre textiles are manufactured and modelled as a stack of layers, in which every layer corresponds to either a combination of fibre textiles and matrix or pure matrix. Each of these layers is then attributed a mechanical response that depends on the constituents of that layer, after which the whole specimen is built up in the thickness by stacking these layers on top of each other. For the fibre textile combinations, two glass fibre textiles with a different density and one carbon fibre textile are considered. The used textiles are schematically shown in Figure 1 to Figure 3. Four different layups combining these fibre textiles are considered and are thoroughly discussed in paragraph 2.1.

The results obtained from a tensile experimental campaign, performed on six specimens of each of the four considered layups (24 specimens in total), are used as an input for the layered-wise numerical model. The layered-wise composite modelling approach is then verified by predicting the flexural mechanical response of bending experiments performed on six specimens for each of the same four layups. All experimental displacement fields are obtained through the Digital Image Correlation technique (DIC), a full field monitoring technique [21].

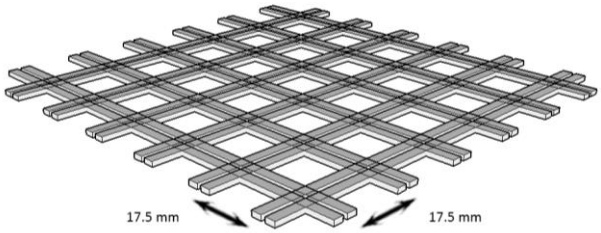

Figure 1: High density 2D glass fibre textile

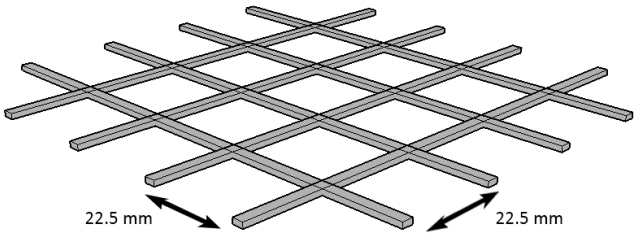

Figure 2: Low density 2D glass fibre textile

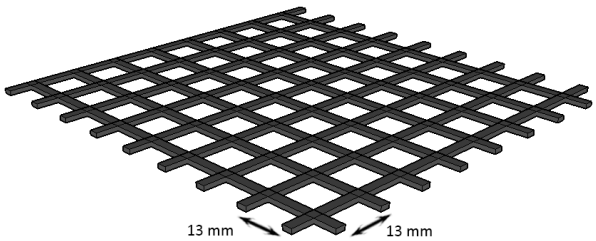

Figure 3: 2D carbon fibre textile

2. Materials and methods

2.1.Used materials

This paragraph will discuss the materials considered in this research. For the matrix, the most important criterion is a high flowability before hardening in order to be able to fully impregnate the fibre textiles. The chosen matrix material is a commercially available grout [22], its properties are listed in Table 1.

Table 1
Properties of the cementitious matrix, obtained from [22]

Aggregate size (mm)	Compressive strength (28d) (MPa)	Bending strength (28d) (MPa)	Density after mixing (kg/m³)	Young's modulus (GPa)
0 - 1.6	55	12	2010.49	9

Two different fibre materials are considered: AR glass and carbon. The first AR glass fibre textile is made of two yarns per mesh as shown in Figure 1, while the other possesses only one yarn per mesh (Figure 2). The fibre textile with two yarns per mesh will from now on be called "high density glass fibre textile" or "HG"; while, the counterpart with only one yarn will be referred to as the "low density glass fibre textile" or "LG". The carbon fibre textile has a relatively smaller mesh size and only one yarn per mesh, it will be referred to as the "C" fibre textile. The main properties of the three fibre textiles are summarized in Table 2, the thickness of the textiles was measured by a calliper as 1.25 mm. All discussed textiles have a styrene-butadiene coating, this coating is external and does not fully impregnate the fibre yarns. The provided stiffness and maximal stress are applicable for the fibre textiles. These values are therefore generally lower than the properties of glass and carbon, since the effect of fibre bundling, loss of impregnation due to coating and textile geometry come into play. The maximum stress values are however experimentally never reached, since fibre pull-out is witnessed as main failure mechanism, as will be discussed in paragraph 4.

Table 2
Properties of fibre textiles, obtained from datasheets [23]–[25]

Name	Code name	Material	Mesh size (mm x mm)	Coated density (g/m²)	Uncoated density (g/m²)	Specific gravity (g/cm³)	Textile stiffness (GPa)	Textile max stress (MPa)
Low density Sitgrid 701	LG	AR-Glass 2400 tex	22.5 x 22.5	308	268	2.68	67	496
High density Sitgrid 200	HG	AR-Glass 2400 tex	17.5 x 17.5	653	568	2.68	67	526
Carbon Sitgrid 017	C	Carbon 48 K	13 x 13	578	516	1.77	93	814

2.2. Considered TRC layups

Two different specimen thicknesses have been chosen, 22 mm and 25 mm. The specimens with a thickness of 22 mm contain 4 fibre textile layers, while the ones of 25 mm contain 6 fibre textiles stacked over the thickness. Figure 4 summarizes the different textile layups considered in this research. The first layup combines the LG and HG fibre textiles in two clusters at a distance of 8.5 mm from each other, with a specimen and cover thickness of respectively 22 mm and 4.25 mm, this layup will henceforth be called "LGHG". The second layup is similar to the first one, except that a second HG layer is added on the top and at the bottom, the total specimen and cover thickness is respectively 25 mm and 4.5 mm and the layup is called "LG2HG". The third considered layup combines the LG textile with the C textile in two different clusters at a distance of again 8.5 mm, this layup is called "LGC". Layup three isn't placed symmetrically over the specimen's thickness, but has a cover of 2.25 mm at the bottom and 6.25 mm at the top. The fourth and last layup adds an extra carbon layer at the top and at the bottom and has a total specimen thickness of 25 mm, it is called "LG2C" with a cover of 2.5 mm at the bottom and 6.5 mm at the top of the specimen, making it also asymmetrical over the thickness. The reason layups 3 and 4 are non-symmetrical is originally related to manufacturing issues. However since the main goal of this research is to investigate a layered-wise modelling approach, a non-symmetrical layup is to be desired as one of the alternative layups.

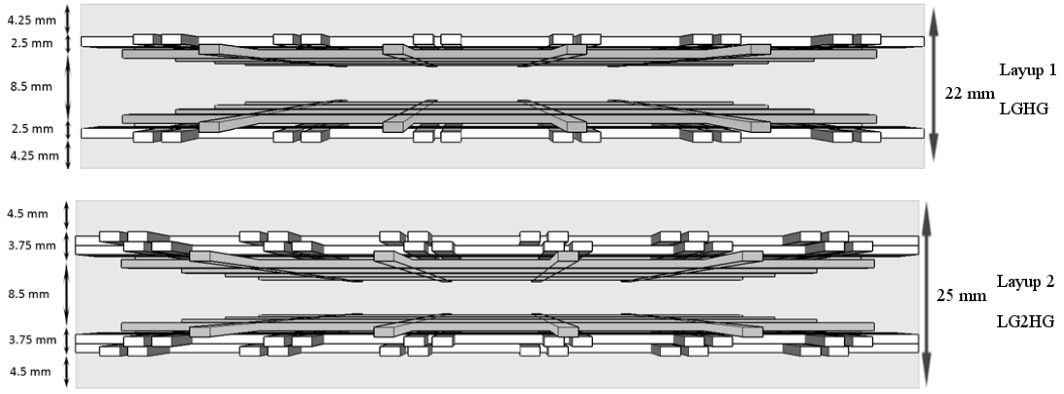

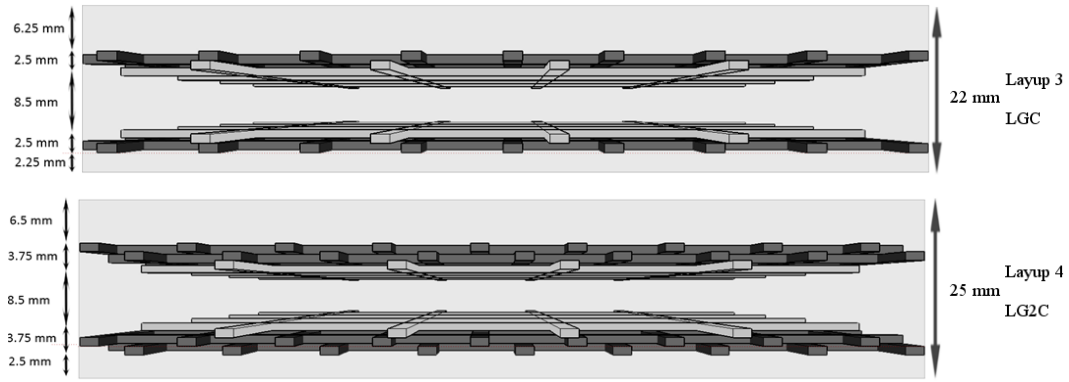

Figure 4: Four different considered fibre textile layups throughout the specimen's thickness: from top to bottom: LGHG, LG2HG, LGC and LG2C

2.3. Specimen manufacturing process

The specimen manufacturing is done by preplacing all the fibre textiles in the mould in the desired layup with the correct spacing, after which the matrix is poured over the fibre textiles until the mould is fully filled. After removing all mortar excess with a flattening ruler, a plastic foil is drawn over the mould. The mould is consequently sealed and the plate is left to harden at room temperature for 28 days. Hereafter the mould is cut in the desired specimen dimensions of 450 mm x 500 mm x 22 or 25 mm, according to [26]. During this cutting process the distance holders for the fibre textiles are cut off in order not to influence the mechanical behaviour of the specimens.

2.4. Tensile & four point bending test setup

The tensile test setup is chosen according to RILEM's TRC tensile test recommendations ([26] - Figure 5). Compared to the RILEM recommendations an extra central pin is added to the clamps to further reduce slippage of the specimen. This through-thickness pin is added because previous experiments without the pin proved to exhibit slippage at the clamps. The addition of the through-thickness pin could induce stress concentrations, but since it is combined with 6 bolts per clamp, tightened by a torque wrench to assure uniform tightening of the specimen, this concentration is neglectable and failure at mid-span of the specimen is observed. Furthermore, rubber sheets are inserted between the clamps and the specimens in order to avoid local stress concentrations and therefore failure at the clamps. The tests are performed on an Instron 5885 test bench with a displacement rate of 1 mm/min.

Digital Image Correlation (DIC), a full field optical monitoring technique [21], offers a full displacement and strain field over the specimens surface during loading. The method works by applying a speckle pattern on the monitored surface of the specimen; this pattern is then captured by means of high-resolution cameras. Any relative displacement of the specimen will result in a strain of the speckle pattern and will therefore be monitored by the technique. This particular experimental campaign was conducted with cameras having a focal length of 17 mm. In order to obtain a high measurement accuracy, extra images were taken in unloaded stage of the specimen and the apparent strains compared to the original image, which had zero strain. The obtained apparent strains were approximately 0.03 %, and therefore neglectable. The acquisition rate adopted was a frame every 70 N or 2 seconds, which resulted in 200 to 300 DIC images per experiment. All the displacements and strains shown in this paper are obtained from the DIC technique, while the load values (and consequently stresses) are directly obtained from the Instron test bench. The final representative strain for the whole specimen was the averaged

strain (at every load step) from several virtual extensometers placed at different positions over the specimen's width within the DIC software. This was done in order to account for the possibility of a crack appearing at one edge of the width; an extensometer placed centrally or at the opposite edge would not be able to record this crack. Hence, by using several extensometers that cover the whole specimen's width, the most representative distribution of the strains is achieved. The gauge length of the extensometers was chosen as the nominal distance between the clamps or supports for respectively the tensile and flexural loading condition, and therefore equal for all experiments.

The four point bending test setup is given in Figure 6. The distance between the supports is 350 mm and between the loads 100 mm. The specimens are tested on the same Instron 5885 at a rate of 2 mm/min. Again, the DIC method is used to obtain the displacements/strains, while the load is obtained directly from the test bench. The DIC cameras can be seen in Figure 6 monitoring the side of the flexural specimen.

Six TRC specimens of each previously discussed fibre textile layup are tested both in tension and in flexure, or thus 24 specimens for each loading state and 48 in total.

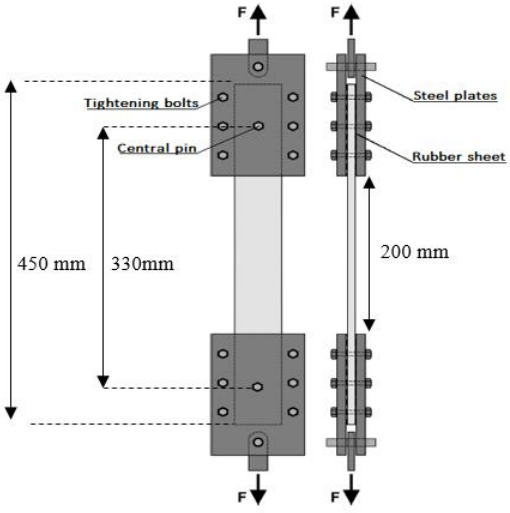

Figure 5: Tensile test setup

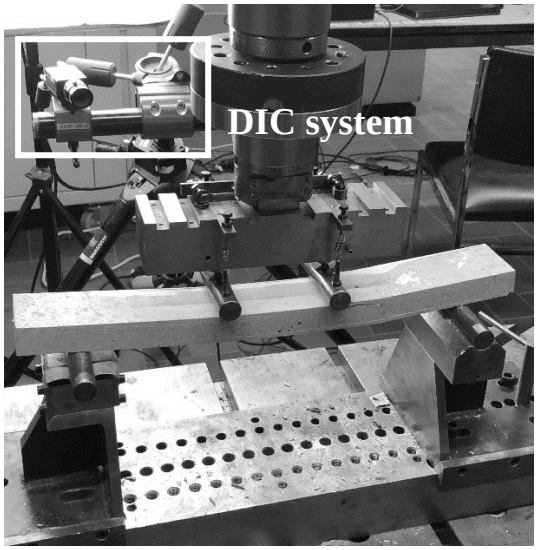

Figure 6: Four point bending test setup

3. Modelling approach

3.1. Theoretical considerations and assumptions

Several assumptions are made in the layered-wise modelling, these will be summarized in this paragraph:

(i) **Layup definition:** All TRC alternatives are subdivided into 5 layers in a similar way: the first and fifth layer are the top and bottom mortar cover layers, the second and fourth layer are the top and bottom textile clusters and the third layer is the mortar layer in the middle (8.5 mm). Layer 2 and layer 4, which represent the layers with combined mortar and textiles, are given a representative thickness of 2.5 mm and 3.75 mm for respectively the layups with two and three fibre textiles per textile cluster, this corresponds to the real thickness of the textiles. The other layers with mortar are given the thicknesses as shown in Figure 4.

(ii) **Tensile properties of the fibre textiles:** In this modelling approach only layers 2 & 4 are assumed to be responsible for the tensile capacity of the entire composite material after the tensile cracking of the matrix. In order to take this into account, the overall mechanical stiffness obtained from the tensile experiments is rescaled to act only on layers 2 & 4. Therefore, the experimental stiffness is multiplied by 4.4 (ratio between the thickness of the total composite to the thickness of the textile layers) in the case of LGHG/LGC, and by 3.33 in the case of LG2HG/LG2C. A typical input curve for the mechanical properties of layers 2 & 4 is given in the orange curve in Figure 7 for the case of the LGHG layup.

(iii) **Tensile properties of the mortar:** The mortar layers are considered to have no further tensile mechanical resistance after the matrix cracking point (around 2.2 MPa). The mortar layers 1, 3 & 5 are therefore given a linear $\sigma - \varepsilon$ behaviour up to matrix cracking, after which their mechanical response remains constant, as can be seen on the blue curve of Figure 7.

(iv) **Compressive properties of the mortar and textiles:** In compression, all the layers are assumed to be linear up to the compressive strength of the mortar (55 MPa).

(v) **Experimental linearization:** Even though the curves obtained from the tensile experiments are not linear, the curves are linearized as a tri-linear tensile behaviour between following points: a) point of zero stress & strain, b) stress & strain (σ_c & ε_c) at the first significant load drop, c) stress & strain (σ_{mc} & ε_{mc}) at the last significant load drop, d) failure stress & strain (σ_f & ε_f). All these experimental stresses and strains composing the tri-linear curve are averaged from the experimental curves and combined as one average tri-linear curve for each layup configuration. An example is shown in Figure 8 for the LGHG specimen. All six experimental curves are plotted in dashed lines in the background for completeness, the used averaged stress-strain curve is represented by the bold continuous black line.

(vi) **Strain/stress behaviour:** The through-thickness strain behaviour of the material is assumed to follow the Euler-Bernoulli's beam theory during all stages of loading (continuous strain distribution), whereas the corresponding stress behaviour depends on the mechanical characteristics given to the considered layer, according to Figure 7.

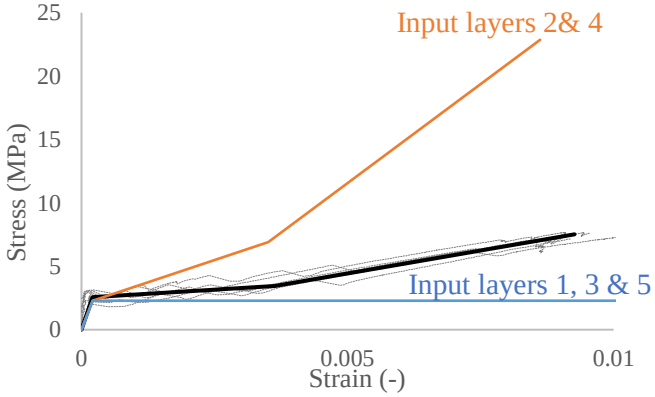

Figure 7: Mechanical curves for different layers of the LGHG TRC layup

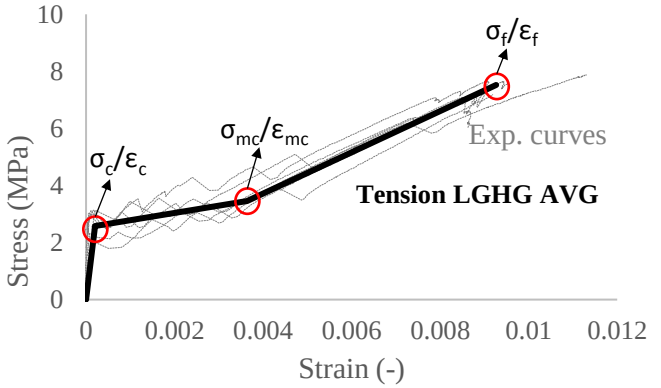

Figure 8: Average experimental tensile tri-linear curve for the LGHG TRC specimen

3.2. Numerical implementation

3.2.1. Material modelling and mesh properties

The model as described in the previous paragraph is implemented implicitly in the finite element modelling software Abaqus [27]. This paragraph will discuss the numerical implementation of the material.

The numerical composite layup is built up in the same way as the layup defined in Figure 4. The mechanical properties are given to the material through a Concrete Damaged Plasticity (CDP) modelling. This CDP model uses a yield function defined by Lubliner [28], taking into account the modifications proposed by Lee & Fenves [29]. Several CDP input parameters are required: the dilation angle, the potential flow eccentricity, the proportion of the ultimate compressive stress in a biaxial test to the uniaxial compressive stress f_{b0}/f_{c0}, the shape of the deviatoric cross-section K and a numerical viscosity parameter. The values of these parameters are summarized in Table 3 and were chosen according to [30]. There should be noted that to improve the convergence of the numerical computation, the viscosity parameter is chosen equal to 0.01 for layers 2 and 4 containing both textiles and matrix material, all other parameters are chosen in the same way as shown in Table 3.

Depending on which layer type is considered (only matrix material or a combination of textiles and matrix), the corresponding mechanical behaviour of Figure 7 is assigned to each layer, and thus a strain hardening tensile behaviour for layers 2 and 4 and a strain softening behaviour for layers 1, 3 and 5.

In the numerical software, the TRC is implemented as a continuum shell. A composite layup is defined onto this shell, meaning all geometrical and mechanical properties have to be defined on the level of the composite layup and are henceforth transferred to the shell. For the meshing of the shell, SC8R shell elements are used, 55 and 8 mesh elements have been chosen in respectively the length and width direction of the specimen as can be seen in Figure 9.

3.2.2. Tensile boundary conditions and loading

For both the tensile and flexural loading condition, a pair of boundary geometrical sets is defined at each extremity of the specimen (BC1 and BC2), this is shown in Figure 9. For tension, a zero displacement boundary condition in the x-direction is attributed to boundary geometrical set BC1. Both boundary condition sets BC1 and BC2 are restrained in the z-direction. Set S1 in Figure 9 is restrained in the y-direction, this is done to ensure symmetry of the displacements. Furthermore, by only restricting the symmetry line of the specimen, Poisson effects are not restrained. The second boundary condition geometrical set (BC2) is constrained to a reference point, to which an x-displacement of 25 mm is imposed, making the modelling displacement controlled, which is in accordance with the experimental campaign. The reaction force and longitudinal displacement are obtained from that reference point and compared to the experimental results.

3.2.3. Flexural boundary conditions and loading

In the case of the flexural loading, a zero displacement in the z-direction is imposed for both geometrical sets corresponding to the supports. Sets S1 and S2 are constrained in respectively the y- and x-direction. The two loading cylinders are implemented as solid elements with an infinite stiffness. These cylinders are constrained to a reference point to which a vertical

displacement of 25 mm is imposed. The reaction force and vertical displacement are obtained from this reference point and compared with the experimental vertical displacement obtained by the DIC at the location of the loading pins. A finite sliding interaction property with frictionless tangential behaviour and hard-contact normal behaviour is defined between the loading pins and the TRC specimen. The displacement is compared at the position of the loading pins because this is a direct history output of the position of the created reference point. Displacement at mid span could also be compared, but yields comparable results.

Table 3
Concrete damaged plasticity parameters for matrix layers 1, 3 and 5

Dilation angle (°)	Eccentricity	f_{b0}/f_{c0}	K	Viscosity parameter
36	0.1	1	0.667	1E-4

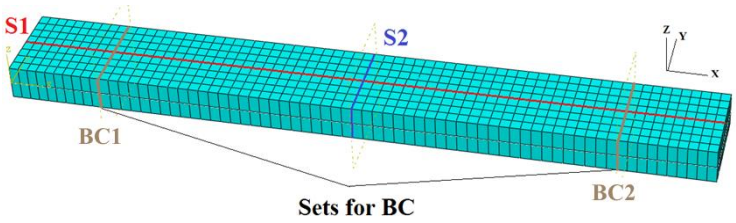

Figure 9: Numerical representation of the TRC specimen

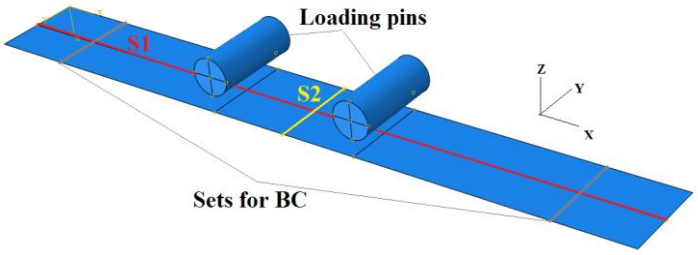

Figure 10: Top view of the bending specimen numerical setup

4. Experimental results & numerical comparison

4.1.Tensile experimental results and numerical comparison

As previously stated, six specimens have been tested in tension for each considered TRC combination given in Figure 4. The results from the experimental campaign will be summarized in this paragraph and compared to the numerical predictions for all combinations in the same way as previously performed in Figure 8.

Figure 11 to Figure 14 give the tensile σ (MPa) – ε (-) response for the LGHG, LGC, LG2HG and LG2C TRC combination respectively. The grey, dashed curves represent the experimental results obtained from the DIC measurements as discussed in section 2.4. The black curves represent the experimental average, obtained as discussed in paragraph 3.1 and the red curves represent the results from the numerical analysis. The numerical stresses are obtained as discussed in paragraph 3.2, by calculating the reaction force on the reference point and dividing it by the cross-section of the specimen.

In tension, a very good agreement can be witnessed between the experimental average and the numerical prediction for all TRC combinations. Keeping in mind that the tensile experimental averages were scaled and inserted only in the thin layers 2 & 4 of the composite layup, the numerical results show the capacity of the model to simulate the global nonlinear strain-hardening behaviour of the entire TRC cross-section in tension, taking into account the rescaling of the mechanical properties before inputting them in layers 2 & 4. Furthermore, it proves the convergence of the modelling approach towards the correct solution since the

simulated stress state is not obtained as a stress directly, but is instead obtained from the reaction force on the reference point divided by the total cross-sectional area of the specimen.

Figure 15 and Figure 16 represent the stress (MPa) and strain (-) through the specimen thickness (for the LGHG case) obtained from the numerical analysis for a specimen strain of respectively 2E-4 and 0.006. In Figure 15, both stress (2.16 MPa) and strain (2E-4) are constant over the specimen thickness since the tensile strength value of 2.2 MPa of the mortar layers has not yet been reached. Once the tensile strength value is reached in the mortar layers, the stress in these layers remains constant at σ_c (2.2 MPa) while it increases in the layers combining mortar and textiles in order to guarantee an equilibrium of forces, resulting in a "double-pillar like" tensile response (Figure 16). At this displacement stage the stress level in the mortar layers is 2.2 MPa and 15 MPa in the textile layers, while the strain level remains constant at 0.006 throughout the specimen's thickness.

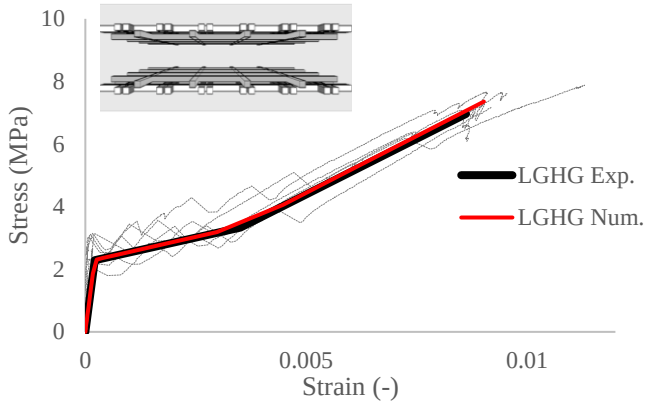

Figure 11: Tensile stress (MPa) – strain (-) curve LGHG: experimental curves, averaged curve and numerical simulation

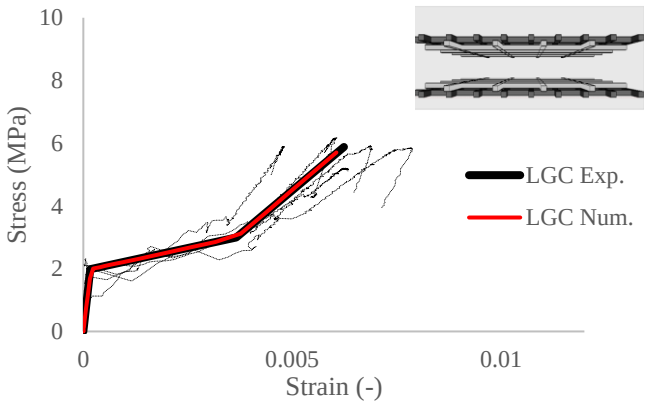

Figure 12: Tensile stress (MPa) - strain (-) curve LGC: experimental curves, averaged curve and numerical simulation

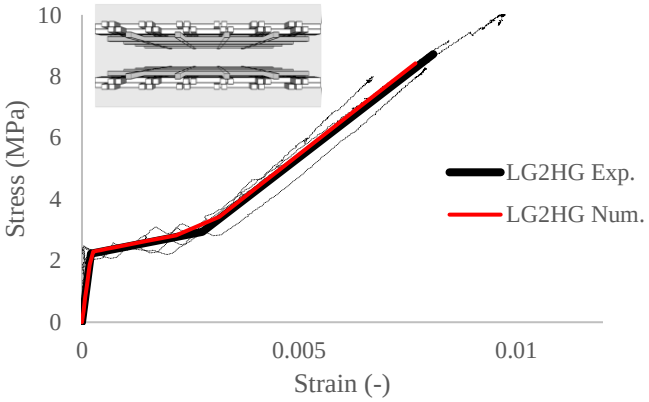

Figure 13: Tensile stress (MPa) - strain (-) curve LG2HG: experimental curves, averaged curve and numerical simulation

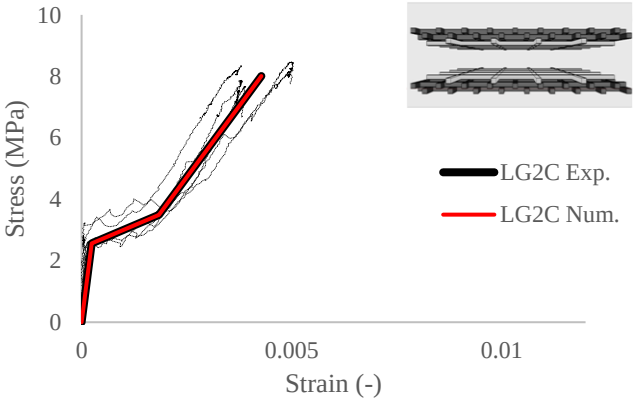

Figure 14: Tensile stress (MPa) - strain (-) curve LG2C: experimental curves, averaged curve and numerical simulation

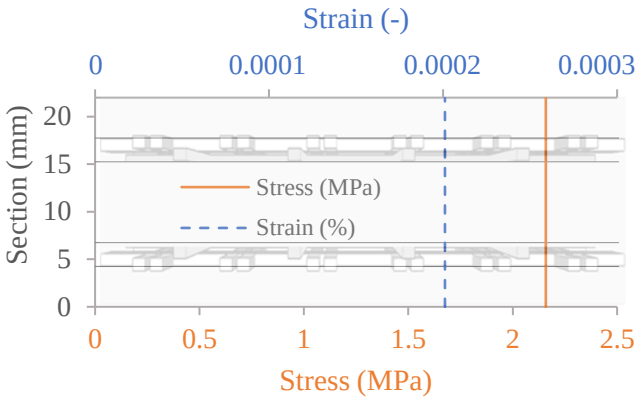

Figure 15: Through-thickness(vertical axis): strain (-) (top axis) and stress (MPa) (bottom axis))distribution in tension for a strain of 2E-4 (LGHG)

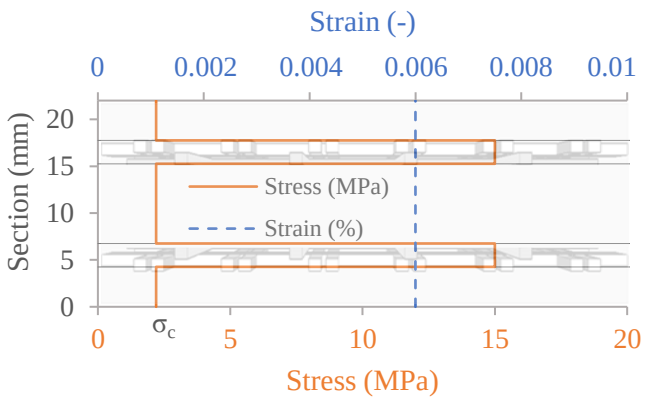

Figure 16: Through-thickness (vertical axis): strain (-) (top axis) and stress (MPa) (bottom axis) distribution in tension for strain of 0.006 (LGHG)

4.2. Flexural experimental results and numerical comparison

In Figure 17 to Figure 20, all flexural experimental curves (six per TRC combination), the averaged experimental curve and the numerical prediction are represented. A good agreement can be witnessed between the experimental results and the numerical predictions for all TRC combinations. This agreement proves the validity of the numerical model for the prediction of the flexural behaviour of TRC, using only the experimental tensile stress-strain curves, the compressive stress at failure and the composite layup as input for the flexural model. All curves behave linear in the first stage, where both the matrix and the textile layers are responsible for carrying the load. When the tensile strength of the matrix is reached in the matrix layers, the stress in these layers remains constant at σ_c (2.2 MPa) and the additional stress is redistributed over the textile layers. A stiffness decrease can be witnessed at this redistribution point. A third stage is distinguished at higher load levels where the stiffness decreases again up to specimen failure, this will further be discussed in the next paragraph. In general, the numerical model predicts the post cracking stage of the TRCs more stiff than the experimental campaign. This difference in stiffness is however not significant and can be attributed to the fact that slight imperfections might have occurred during the specimen manufacturing and therefore the fibre textile's actual positioning throughout the specimen's thickness. In general, the specimens in the flexural loading condition failed due to pull-out of the fibre textiles.

Figure 21 to Figure 23 give an overview of the through-thickness stress (MPa) and strain (-) obtained from the numerical bending analysis at respectively 6E-5, 0.002 and 0.006 maximum strain at the bottom of the section, for the LGHG layup. At 6E-5 maximal strain, the achieved stress in the TRC cross-section does not exceed the tensile cracking stress of the mortar σ_c (2.2 MPa), resulting in a linear through-thickness response of both the strain and the stress (Figure 21). In Figure 22, at 0.002 maximal strain, the maximum tensile stress in the cross-section equals 3 MPa. The through thickness strain response remains linear, as well as the compressive stress response. The tensile stress response however, remains constant at σ_c (2.2 MPa) in the mortar layers which passed the matrix cracking stage. A "pillar-like" peak is witnessed in the layer where a combination of matrix material and fibre textiles are present. This is a direct result of the stress increase in the fibre textile layers due to the constant stress in the mortar layers, since the total load in tension should remain the same. Furthermore, a slight shift of the neutral axis towards the top of the cross-section can be witnessed. This neutral axis shift is required to guarantee the moment equilibrium of the tensile and compressive forces acting on the cross-

section. In Figure 23, at higher strain values of 0.006 maximally, the tensile stress response of mortar layers 1 & 3 is equal to σ_c (2.2 MPa). In order to guarantee moment equilibrium, the neutral axis shifts towards the top, past the second textile layer that was originally in compression. A second pillar tensile stress peak can therefore be witnessed in layer 2. The ratio between these two stress pillar values is the same as the strain values in these layers. Lastly, the point where the tensile stress switches to a compressive stress always corresponds to the point of zero strain throughout all loading conditions.

There should be noted that for the tensile response of the TRC the position of the fibre textiles, and thus the fibre textile layers inside the numerical model, is less critical for the model, since the strain value is constant over the cross-section. For the flexural loading case however, this position is very important, since the total moment carried by the tensile layer is linearly dependent on the distance between the neutral axis and the textile layer. A very precise manufacturing and correct model implementation are therefore crucial parameters for the analysis, since a small difference between the model and the reality can cause a discrepancy between the numerical simulations and experimental results.

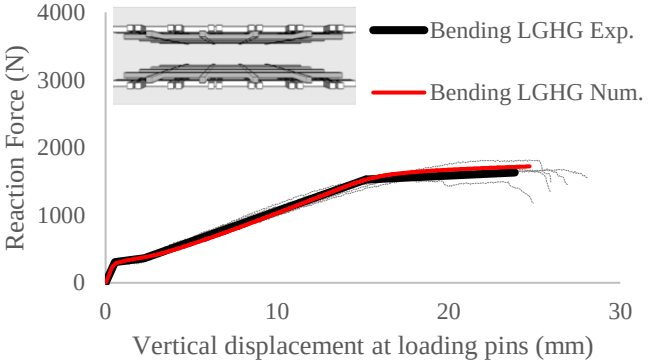

Figure 17: Flexural Force (N) - Displacement (mm) curve LGHG: Experimental curves, averaged curve and numerical simulation

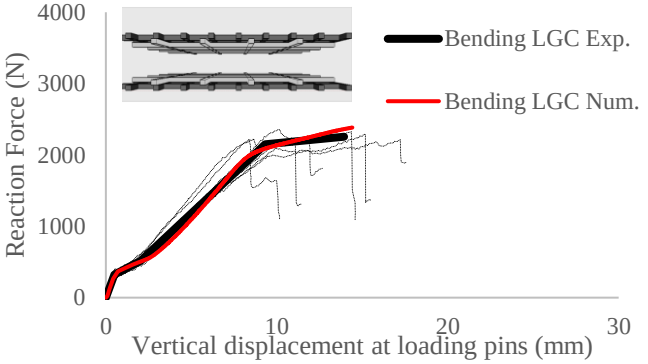

Figure 18: Flexural Force (N) - Displacement (mm) curve LGC: Experimental curves, averaged curve and numerical simulation

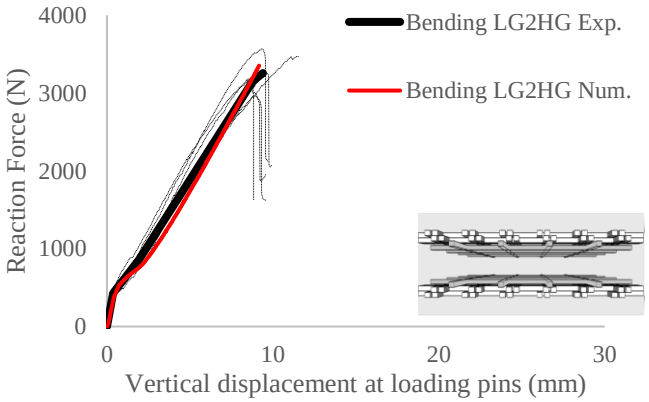

Figure 19: Flexural Force (N) - Displacement (mm) curve LG2HG: Experimental curves, averaged curve and numerical simulation

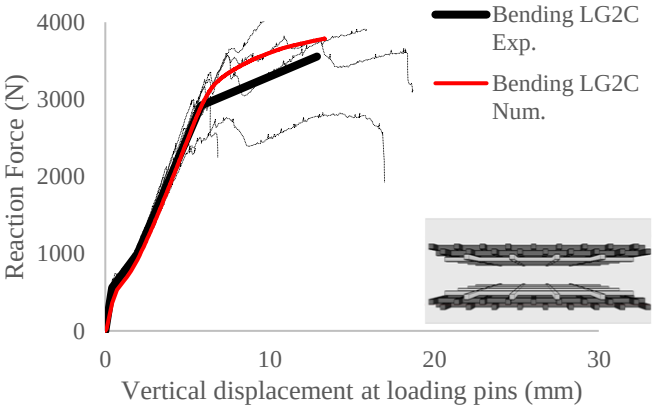

Figure 20: Flexural Force (N) - Displacement (mm) curve LG2C: Experimental curves, averaged curve and numerical simulation

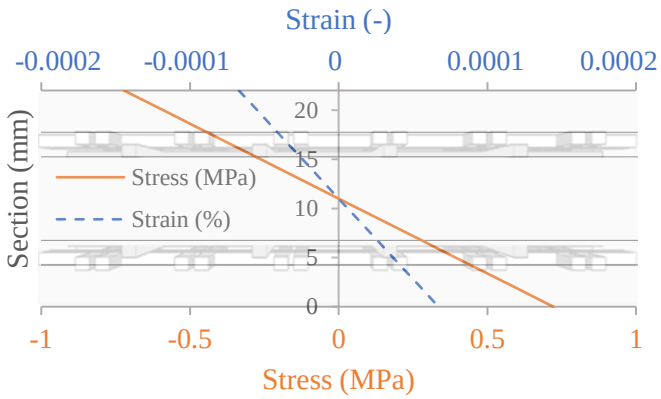

Figure 21: Through-thickness (vertical axis): strain (-) (top axis) and stress (MPa) (bottom axis) distribution at the loading pins for a maximal bottom strain of 6E-5 (LGHG)

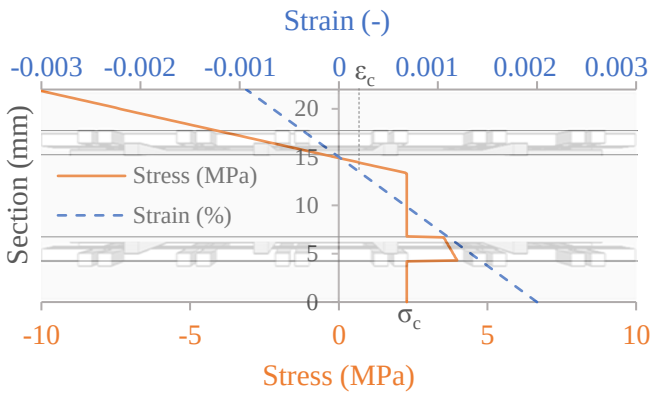

Figure 22: Through-thickness (vertical axis): strain (-) (top axis) and stress (MPa) (bottom axis) distribution at the loading pins for a maximal bottom strain of 0.002 (LGHG)

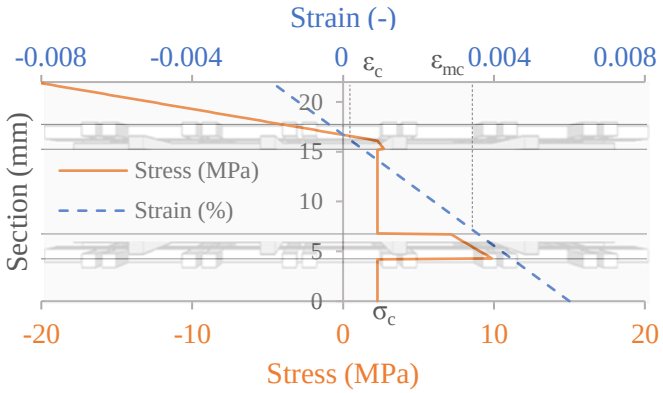

Figure 23: Through-thickness strain (-) and stress (MPa) distribution at the loading pins for a maximal bottom strain of 0.006 (LGHG)

5. Conclusions

A layered wise modelling approach for TRCs is presented in this paper. The tensile response after matrix cracking is assumed to be only carried by layers where fibre textiles are present and the mechanical response of the whole cross section is rescaled and attributed to these textile layers.

An experimental campaign consisting of both tensile and bending tests validate this modelling approach. A good agreement between the experimental results and the numerical modelling is witnessed. In the tensile loading case, the layered wise modelling approach results in a "double-pillar like" response through the specimen thickness. For the flexural loading case an evolving through-thickness stress behaviour is witnessed, while a linear strain response is preserved. The stress behaviour evolves according to whether or not the tensile matrix strength is reached in the mortar layers. The stress in the textile layers consequently adapts to carry the applied load and the neutral axis shifts in order to guarantee moment equilibrium throughout the cross-section.

This paper proves that a layered wise numerical model, allowing for an accurate lever arm simulation of TRC's discretely reinforced over the cross section, yet without the need for integrating the bond properties between the fibre textiles and the matrix material in the model, can be used to predict the bending behaviour of TRCs.

Acknowledgements
The work performed in this paper is made possible by the funding of the Agentschap Innoveren & Ondernemen and is part of a larger SBO-project (CeComStruct). The authors would like to thank all involved parties that made this research possible.

Bibliography

[1] W. Brameshuber, Textile Reinforced Concrete: State of the Art Report, RILEM Technical Commitee 201-TRC, first ed., RILEM Publications, Aachen, Germany, 2006.

[2] A. Bentur, S. Mindess, Fibre Reinforced Cementitious Composites, Modern Cocnrete Technology Series, second ed., Taylor & Francis Group, 2007.

[3] J. Aveston, G. A. Cooper, A. Kelly, Single and multiple fracture, The Properties of Fibre Composites, pp. 15–24, 1971.

[4] T. Triantafillou, Textile Fibre Composites in Civil Engineering, 1st Edition, Woodhead Publishing, 2016.

[5] E. Sharei, A. Scholzen, J. Hegger, R. Chudoba, Structural behavior of a lightweight, textile-reinforced concrete barrel vault shell, Composite Structures, vol. 171, pp. 505–514, 2017.

[6] A. Scholzen, R. Chudoba, J. Hegger, Thin-walled shell structures made of textile-reinforced concrete, Structural Concrete, vol. 16, pp. 115–124, 2015.

[7] E. Verwimp, T. Tysmans, M. Mollaert, S. Berg, Experimental and numerical buckling analysis of a thin TRC dome, Thin-Walled Structures, vol. 94, pp. 89–97, 2015.

[8] R. Chudoba, W. Graf, K. Meskouris, Numerische Modellierung von textilbewehrtem Beton, John Wiley Sons, vol. 99, no. 6, pp. 460–465, 2004.

[9] M. Mombartz, J. Hegger, R. Chudoba, and F. Peiffer, Simulation of textile reinforced concrete with 2D discrete crack and discrete crack bridges representation, Computational Modelling of Concrete Structures - Proceedings of EURO-C 2006, pp. 167–172, 2006.

[10] E. Bertolesi, F. G. Carozzi, G. Milani, C. Poggi, Numerical modeling of Fabric Reinforce Cementitious Matrix composites (FRCM) in tension, Construction and Building Materials, vol. 70, pp. 531–548, 2014.

[11] Z. I. Djamai, M. Bahrar, F. Salvatore, A. Si Larbi, M. El Mankibi, Textile reinforced concrete multiscale mechanical modelling: Application to TRC sandwich panels, Finite Element Analysis and Design, vol. 135, pp. 22–35, 2017.

[12] G. Mazzucco, T. D'Antino, C. Pellegrino, and V. Salomoni, Three-dimensional finite element modeling of inorganic-matrix composite materials using a mesoscale approach, Compos. Part B Eng., vol. 143, no. December 2017, pp. 75–85, 2018.

[13] B. Mobasher, V. Dey, Z. Cohen, A. Peled, Correlation of constitutive response of hybrid textile reinforced concrete from tensile and flexural tests, Cement and Concrete Composites, vol. 53, pp. 148–161, 2014.

[14] N. Williams Portal, K. Lundgren, A. M. Walter, J. O. Frederiksen, L. N. Thrane, Numerical modelling of textile reinforced concrete, Proceedings of the 8th

International Conference on Fracture Mechanics of Concrete and Concrete Structures FraMCoS, pp. 886–897, 2013.

[15] R. Chudoba, E. Sharei, A. Scholzen, A strain-hardening microplane damage model for thin-walled textile-reinforced concrete shells, calibration procedure, and experimental validation, Composite Structures, vol. 152, pp. 913–928, 2016.

[16] I. G. Colombo, M. Colombo, M. di Prisco, F. Pouyaei, Analytical and numerical prediction of the bending behaviour of textile reinforced concrete sandwich beams, J. Build. Eng., vol. 17, no. February, pp. 183–195, 2018.

[17] T. Tysmans, M. Wozniak, O. Remy, J. Vantomme, Finite element modelling of the biaxial behaviour of high-performance fibre-reinforced cement composites (HPFRCC) using Concrete Damaged Plasticity, Finite Elements in Analysis and Design vol. 100, pp. 47–53, 2015.

[18] A. Peled, R. Haik, E. A. Sasi, Influence of three-dimensional (3D) fabric orientation on flexural properties of cement-based composites, Cement and Concrete Composites, vol. 80, 2017.

[19] M. El Kadi, S. Verbruggen, J. Vervloet, M. De Munck, J. Wastiels, T. Tysmans, Experimental investigation and benchmarking of 3D textile reinforced cementitious composites, 4th International Conference of Strain-Hardening Cementitious Composites, pp. 1–8, 2017.

[20] A. E. Naaman, Textile Reinforced Cement Composites: Competitive Status and Research Directions Ferrocement, in International RILEM Conference on Material Science, 2010, vol. I, pp. 3–22.

[21] M. A. Sutton, J.-J. Orteu, H. W. Schreier, Image correlation for Shape, Motion and Deformation Measurements. Springer, 2009.

[22] Sika, Sikagrout 217, Note de produit, https://fra.sika.com/dms/getdocument/sikagrout 217_nt810.pdf, 2016.

[23] V. Fraas, Technical Datasheet SitGrid701, www.solutions-in-textile.com, 2017.

[24] V. Fraas, Technical Datasheet SitGrid200, www.solutions-in-textile.com, 2017.

[25] V. Fraas, Technical Datasheet SitGrid017, www.solutions-in-textile.com, 2017.

[26] W. Brameshuber, Uniaxial Tensile Test: Test Methods and Design of Textile Reinforced Concrete, RILEM Technical Committee, 2016.

[27] Simulia, Abaqus Theory Manual and Users' Manual, Version 6.12, Hibbit, Karlsson & Sorenson, INC., 2006.

[28] J. Lubliner, J. Oliver, S. Oller, E. Onate, A plastic-damage model for concrete, J. Solids Structures, vol. 25, no. 3, pp. 299–326, 1989.

[29] J. Lee, G. L. Fenves, A plastic-damage concrete model for earthquake analysis of dams, Earthquake Engineering and Structural Dynamics, vol. 956, pp. 937–956, 1998.

[30] M. Wozniak, T. Tysmans, S. Verbruggen, J. Vantomme, Nonlinear indirect identification method for cement composite-to-concrete bond, Composite Structures, vol. 176, pp. 72–81, 2017.